ISTITUTO NAZIONALE DI RICERCA METROLOGICA
Repository Istituzionale

Metrological Evaluation of the Building Influence on Air Temperature Measurements

(Article begins on next page)

24 November 2024

Article

Metrological Evaluation of the Building Influence on Air Temperature Measurements

Carmen Garcia Izquierdo [1,*], **Graziano Coppa** [2], **Sonia Hernández** [1] **and Andrea Merlone** [2]

1   Centro Español de Metrología, 28760 Tres Cantos, Spain
2   Istituto Nazionale di Ricerca Metrologica, 10135 Turín, Italy; g.coppa@inrim.it (G.C.)
*   Correspondence: mcgarciaiz@cem.es

Abstract: This paper describes the metrological procedure carried out for the evaluation of the building influence on air temperature measurements. This evaluation aims to produce reliable conclusions, information, and data to contribute to the WMO siting classification schemes for air temperature measurements. For this purpose, a field experiment was designed, deployed, and carried out. As a result, one-year-lasting air temperature measurements were collected and analyzed. In this field experiment, a 200 m wide building is the unique artificial heat source and the unique object projecting shades over a flat surface (no discernible slope) in an open space bigger than 40,000 m^2, covered with short grass. Eight calibrated thermometers, equipped with the same model of artificially ventilated radiation shields, were set up at a height of 1.5 m from the ground and at different distances from a 200 m wide building. This configuration provides the observation of the horizontal air temperature radially distributed from the building and, as a conclusion, it enables the quantification of the building influences on air temperature measurements at different distances from the building. This document describes the field experiment, the analysis procedure, the evolution of the building influence on air temperature measurements along the day, and the impact of other meteorological parameters on this building effect. Two different building effects are observed: the positive building effect, where the air temperature decreases with the distance to the building, and the negative building effect, where the air temperature increases with the distance to the building. It is also noticed that the building influence is higher on clear days and the daily maximum building influence values are directly linked with the corresponding maximum solar irradiance. The influence of wind on the building effect is also analyzed, reaching the conclusion that due to characteristic of local winds, in terms of low speed and direction, the wind impact could be considered as negligible. The maximum values of building influence on air temperature measurements, the associated uncertainty analysis, and the conclusions are presented in this paper. All these points have been addressed using metrological principles with the purpose of giving consistency and robustness to the evidence presented here.

Keywords: air temperature measurements; siting classification; building influence on air temperature measurements; uncertainty of air temperature measurements; metrology for meteorology and climate

1. Introduction

The quality and representativeness of the near ground air temperature measurements, besides other factors, strongly depend on the environmental conditions of the measurement site itself. The temporary variation in the site conditions, mainly due to the urbanization of the area surrounding the thermometers, could generate inhomogeneities in the observed temperature data and, hence, lack of robustness and representativeness in the climate evolution study. This fact is highlighted in the WMO No. 8 Guide [1], where a siting classification for surface observing stations on land is defined.

This classification works as the surrounding area representativeness index where the measurements are taken. It simplifies the metadata associated with the measurements,

allowing more suitable and more direct comparisons between measurements taken in different locations and at different times.

Five classes for surface observations are established [1], where a lower classification number means that the corresponding measurements are representative of a wider area and the effects of surrounding obstacles are lower. According to this siting classification for surface observation stations on land [1], the main factors adversely affecting air temperature measurements are unnatural surfaces and shades. Their impacts on the measurements could imply higher errors and/or uncertainties [2,3] than the ones due to the measurement instrument itself. The proximity of the thermometers to different types of obstacles, such as buildings, roads, water sources, or trees, implies the ground air temperature measurements are more affected by these obstacles [1,4–10]. In this context, and considering the limited knowledge about how and at what extent nearby heat sources affect air temperature measurements in real settings, some works have been carried out [4–10]. Despite this fact, some information and conclusions are still missing. With the aim of reducing this lack of knowledge, experiments with a strong metrological background have been performed in the frame of the European project EMRP ENV58 MeteoMet2 [8], where one-year-lasting field experiments were designed and implemented to study the influence of roads [9], trees, and buildings on air temperature measurements.

The main scope of this study is to support the WMO in improving the present siting classification scheme [1]. The research work presented here analyses air temperature measurements affected by a unique influence, a building, and this building impact is quantified as a function of the distance to the building. Firstly, a very specific field experiment was designed and implemented, where the building and the surrounding area played a fundamental role. A set of thermometers were deployed at several distances from the building, fulfilling the different classes defined in the WMO siting classification [1]. The instrumentation used in this experiment was calibrated [2] and all of the measurements are traceable [2] to the International System of Units [11]. Measurements of this one-year-lasting experiment were studied and analyzed. This paper describes the daily systematic, repetitive, and consistent building effects on air temperature measurements. The building effect values and evolutions are also studied as a function of the daily meteorological conditions. In the analysis presented here, the aleatory effects are removed from the study.

By using all of the one-year measurements, the evolution of the building influence on air temperature measurements throughout the day is stablished. In addition, the impact on the building influence of several meteorological quantities, like wind, solar irradiance, and air temperature, have been studied for the quantification of the maximum building influence on air temperature measurements. Additionally, the associated uncertainty of these values is discussed, explained, and quantified, giving ideas about the robustness of the measurements and the control limits of the experiment.

Previously to the research described here, different investigations were performed where the air temperature and buildings were combined [10,12–17]. Some of these works [12–17] are more focused on studying Urban Heat Islands and the involvement of several buildings (of different sizes and materials) and the involvement of additional impact factors, such as roads. These works are more related to understanding the heat storage capacity of buildings and pavements and its impact on urban microclimates. Instead, this work deals with air temperature in clean and open environments and with a unique building as the influencing factor. As a consequence, the procedures followed in this research work presents differences regarding the ones focused on Urban Heat Islands.

The activities performed in [10] follow a similar strategy to the one proposed in this paper, with the difference that a cluster of buildings and paver surfaces were considered in [10]; meanwhile, a bigger building is the unique influencing factor on air temperature measurements in this study. In addition to this, the solar orientation of the buildings in [10] is different than in this research work, giving different but linked conclusions as a result.

It is expected that the WMO siting classification for ground-based air temperature measurements will benefit from the results of this field experiment, which has been designed

under metrological principles to provide thoroughness, accuracy, robustness, and comparability to all measurements. The involvement of metrology aims to provide the real limits (in terms of uncertainties) of the conclusions presented here. In addition to this, the procedure proposed in this work could be considered as one pillar for measurement procedures in future experiments on siting classifications. The use of common measurement procedures in different siting experiments will allow the comparison and combination of the conclusions developed in future works. The work proposed here can contribute to addressing temporal stability issues in climate monitoring, including the quality control and homogenization of air temperature records to be considered in reference climate networks [10].

2. Method, Materials, and Field Experiment

The field experiment described in this paper has the aim of quantifying a building's impact on air temperature measurements.

In this field experiment, eight calibrated thermometers, equipped with the same model artificially ventilated radiation shields, were set up at a height of 1.5 m from the ground and at different distances from a 200 m wide building (Figures 1 and 2). This layout enables the observation of the horizontal air temperature distribution, radially from the building. The air temperature measurements were continuously monitored for one year to detect the variation in building influence on air temperature across a large range of meteorological conditions.

2.1. Instrumentation

Air temperature; air humidity; wind speed; wind direction; and solar irradiance were measured in this research work.

For air temperature measurements, identical thermometers were used: four wire platinum resistance thermometers, Pt-100 (IEC-751, Class 1/10 DIN) [17], assembled by the same manufacturer. They were encapsulated in a stainless-steel sheath and their dimensions were 6 mm diameter and 60 mm long. These thermometers were calibrated in liquid baths [18,19] with traceability to the International Temperature Scale of 1990 (ITS-90) [20]. The expanded uncertainty ($k = 2$) [3] associated to the calibration of the thermometers was 0.01 °C and the drift [2] of the thermometers was determined by the calibration of the thermometers before and after the external exposure. The drift was lower than 0.02 °C for all the thermometers. The thermometers' drift are low enough to not impact on the air temperature measurements taken along the field experiment life and for hence, on the conclusions of this paper. Nevertheless, the source uncertainty due to the drift of the thermometers is included in the total uncertainty budget (Section 3.5).

In order to mitigate the influence of solar radiation and rain on the air temperature measurements, each thermometer was mounted inside an active ventilated radiation shield, all of the same model: Young mod. 43502. The manufacturer states that the maximum error in air temperature measurements due to solar irradiance is lower than 1% under a flux of 1000 W/m^2.

The air humidity was measured using a Hygrometer model ETM-30 by Lombard & Marozzini (Rome, Italy) with an accuracy of 1%, in agreement with manufacturer specifications. The hygrometer was mounted inside a multi-plate solar radiation shield at a height of 1.5 m above the ground.

The solar irradiance was monitored using a radiometer, Hukseflux LP02 (Delft, Netherlands), whose specifications say that it measures solar irradiance in the range of 0–2000 W/m^2 with an expanded uncertainty ($k = 2$) lower than 1.8%.

Wind speed and wind direction were measured using a 2D sonic anemometer (Gill Wind, model WindSonic 75, Hampshire, UK), whose manufacturer specifications state that it measures wind speed in the range of 0–60 m/s with an accuracy of $\pm$2% at 12 m/s and a response time of 0.25 s. The sonic anemometer was set at 2.5 m high above the ground.
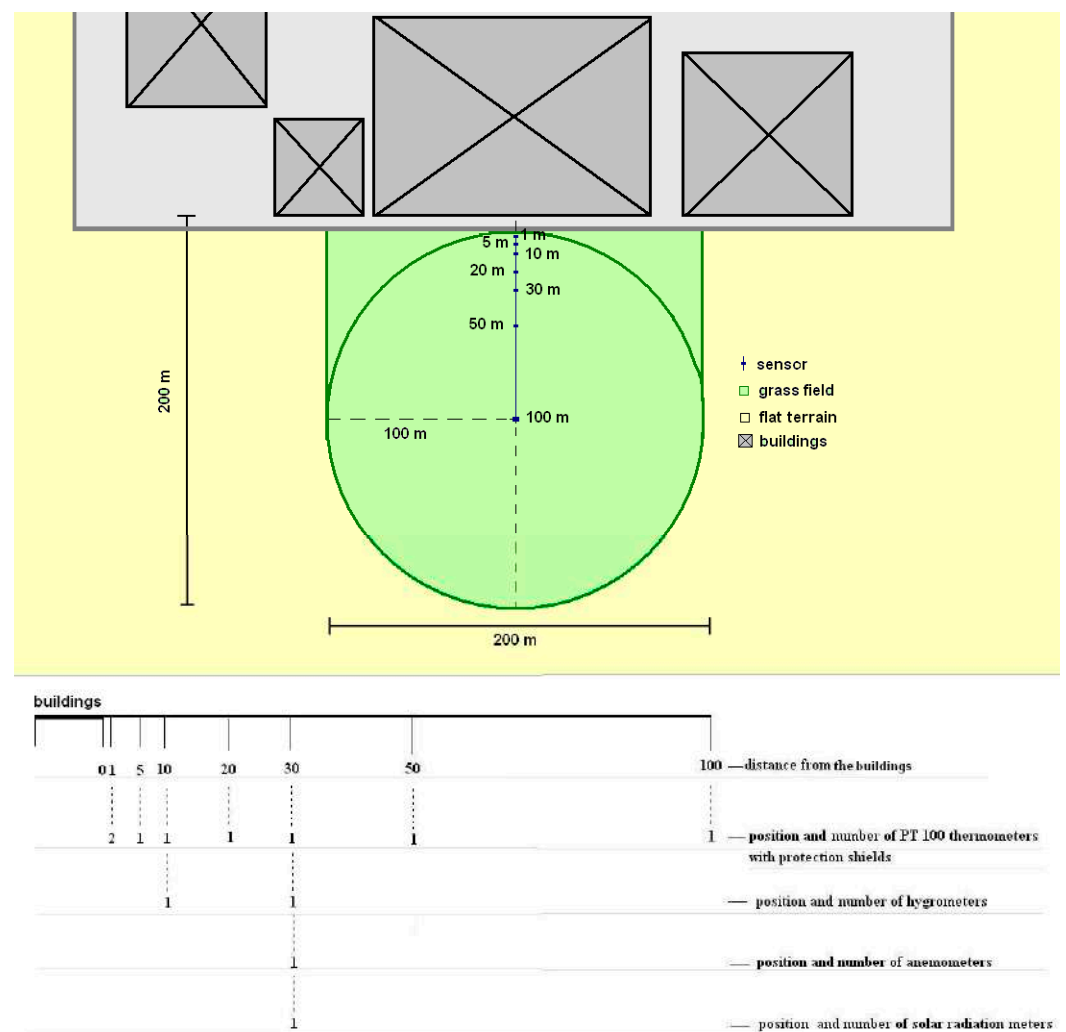
Figure 1. Design of the field experiment with the requirements about distances (in meters) and with the positions of the different poles where the different instrumentation is installed. A flat area of 4×10^4 m^2 is free of obstacles, with the exception of a building (or set of buildings). The reference temperature of the experiment is provided by a thermometer sited at 100 m from the building. The building effects (at several distances from the building, Table 1) are evaluated using the difference in the thermometer readings (placed at the different distances from the building, Table 1) regarding the reference temperature (100 m).

Table 1. WMO siting classification [1] of the thermometers placed at the different poles.

	Pole 1	Pole 2	Pole 3	Pole 4	Pole 5	Pole 6	Pole 7
Distance to the building	1 m	5 m	10 m	20 m	30 m	50 m	100 m
Class due to the distance to the building	4	4	3	3	2	2	1
Class due to distance to the building and due to the shadow of the building on the thermometer	5	5	4	4	2	2	1

A common dedicated datalogger recorded the measurements of all of the instrumentation. The expanded uncertainty associated with the readings of the thermometers in the datalogger was 0.05 °C ($k = 2$).

Figure 2. Real aerial view (©Google, 2016) of the selected site. The sensors are positioned along the red line, with a total length of 100 m, as described in the lower panel of Figure 1. The reference thermometer is placed at 100 m from the building. The blue arrow indicates the direct of north.

2.2. Field Description

A thorough search of the appropriate location for this experiment was conducted in order to obtain robust and useful conclusions from the experiment. The selected place is located in Spain: 40°38′ N, 4°44′ W. It is a flat surface (no discernible slope), an open space bigger than 40,000 m^2, covered with short grass and without any artificial heat sources or objects projecting shade over the instrumentation, with the exception of the building.

Figure 1 shows the layout of the experiment with the arrangement of the instrumentation, while Figure 2 displays an aerial view of the real experiment place where the red line represents the 100 m long path where the poles, with the different instrumentation, were deployed at different distances from the building.

The building—6 m tall and 200 m wide—is approximately oriented to the northwest/southeast direction. The walls of the building are made of concrete painted in white, as Figure 3 shows. The surrounded area is covered by natural grass, without any ground pavement surrounding the building.

Periodic maintenance of the area was performed in order to fulfil the requirements established by WMO Guide No. 8 [1] for Class 1 air temperature measurements.

2.3. Deployment of the Instrumentation on Field

The instrumentation was arranged at seven sampling points (poles), distributed radially and perpendicularly to the building and at different distances from it: pole 1 is at 1 m from the building, pole 2 at 5 m, pole 3 at 10 m, pole 4 at 20 m, pole 5 at 30 m, pole 6 at 50 m, and pole 7 at 100 m from the building (Table 1). The involved instrumentation was distributed as is it described in Figure 1.

The thermometers were installed at 1.5 m height from the ground and facing south in order to avoid the shadow of the pole on the thermometers (Figure 4). Two thermometers were installed in pole 1; one of them was placed to the north side and the other one to the south so that both thermometers were at the same distance from the building (1 m). This redundant measurement system in pole 1 was included as an assurance that the experiment

would provide useful measurements and also in case one of the thermometers in pole 1 failed during the infield exposure.

Figure 3. View of the wall of the building.

Figure 4. View of the thermometers from the wall of the building.

The radiometer and sonic anemometer were installed following the recommendations of the manufacturers. The radiometer was installed at 2 m high and was south facing in order to avoid the shadow effect of the pole. The sonic anemometer was placed 2.5 m high. The wind's blowing direction provided by the sonic anemometer followed the orientations, regarding the building, provided in Table 2.

With the exception of the building, the field around the sensors was free of any obstacles in a radius of 100 m. In particular, the thermometer at pole 7 (the one at 100 m) is a Class 1 according to WMO siting classification [1] and its readings are considered as the reference temperature.

Table 2. Relationship between the wind's blowing direction and the position of the building.

Measurement of Sonic Anemometer Direction in °	Wind's Blowing Direction
0, 360	From north to south in parallel with the building.
90	From east to west, perpendicular to the building, flowing from the building to the thermometers.
180	From south to north in parallel with the building.
270	From west to east, perpendicular to the building, flowing from the thermometers to the building.

3. Experimental Results and Discussion

The analysis of the building influence on air temperature measurements is performed via the study of the air temperature variations at poles 1 to 6 in comparison to the air temperature variation at the reference point (pole 7). The quantity Δt_i, called "building influence" in this paper, is defined as follows:

$$\Delta t_i = t_i - t_7 \tag{1}$$

where t_i and t_7 are the temperatures at the sampling point (pole i) and at the reference point (pole 7), respectively.

The aim of this study was to find the maximum values of building influence. As is explained later in this paper, two building effects have been observed: positive building influence and negative building influence, following Equations (2) and (3), respectively:

$$\Delta t_{imax\text{-}positive} = max(\Delta t_i) = max(t_i - t_7), \tag{2}$$

$$\Delta t_{imax\text{-}negative} = min(\Delta t_i) = min(t_i - t_7). \tag{3}$$

3.1. Anthropogenic Impact of Building on Air Temperature

The selected building is a biscuit factory with several furnaces inside it. Due to this fact, the first analysis had the aim to evaluate the influence of this human activity on the air temperature measurements at pole 1 (1 m from the building). For this purpose, the difference between the building influence at pole 1 during the working days (Monday to Friday) and during the weekends (Saturday and Sunday) was analyzed. Figures 5 and 6 show examples of the reference temperature (pole 7) and the building influence at pole 1 for the complete weeks.

In order to perform a robust study about the effect of human activity on building influence, it was necessary to choose the appropriate weeks where the meteorological conditions along the complete week were very similar, meaning the human activity was the unique impacting factor on the evolution of the building influence. From the complete set of data collect across 52 weeks, 2 weeks were selected that had daily reference temperatures that were very similar throughout each day of the week. In addition, all the days were totally clear, without clouds, and the maximum values of solar irradiance were very similar for each of the days. Figures 5 and 6 include the information of the two chosen weeks, both of them with very stable meteorological conditions along each of the weeks and with a solar irradiance of $\approx$500 W/m^2 for the week of December (Figure 5) and with $\approx$1000 W/m^2 for the week of August (Figure 6). These solar irradiance values are one of the highest and one of the lowest observed along the complete year of measurements. In these two selected weeks, the change in human activity (between working and no-working days) could be considered as the unique impacting factor on building influence. This analysis and quantification is based on repetitive air reference temperature conditions along the week and for the solar irradiance range observed in this study. This last point is important since, as it is established later in this paper, the factor with the highest impact on the building influence is solar irradiance. In Figures 5 and 6, the black line represents the building

influence at pole 1; meanwhile, the grey line represents the evolution of the reference air temperature at pole 7.
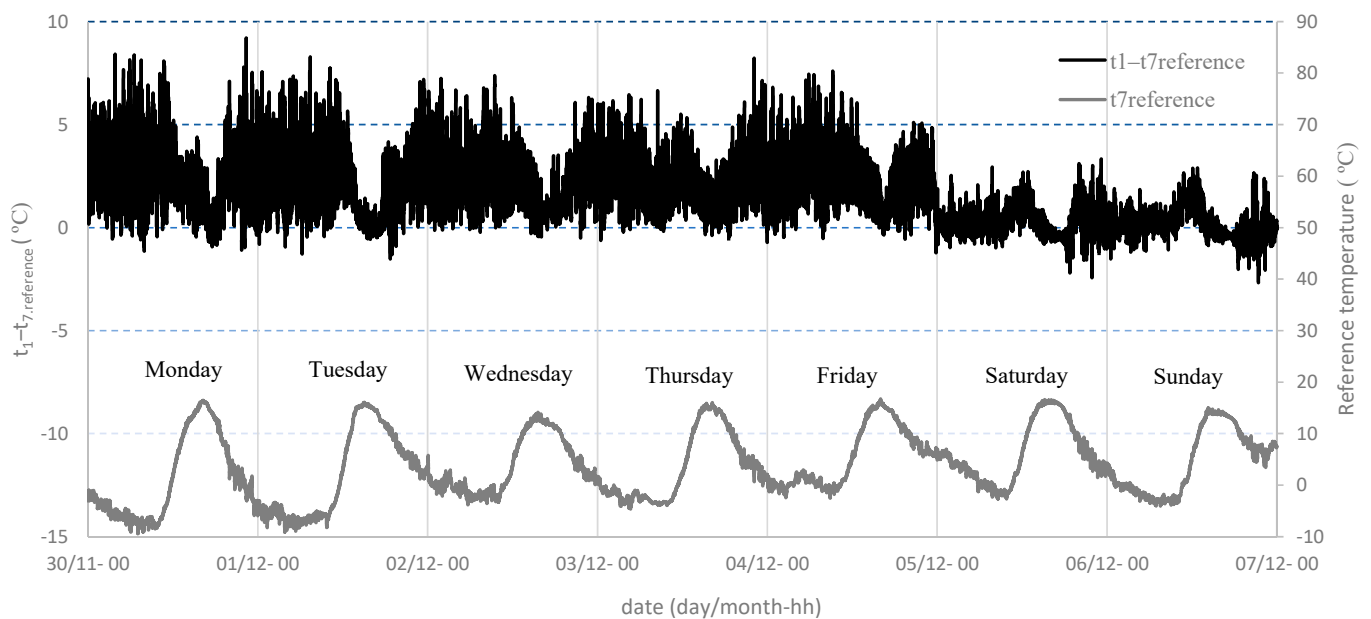

Figure 5. Reference temperature (grey line) and building influence (black line) at pole 1 for a complete week. Data obtained for sunny days with a daily maximum solar irradiance ~500 W/m^2. Working days (Mo–Fr) and weekends (Sa–Su).
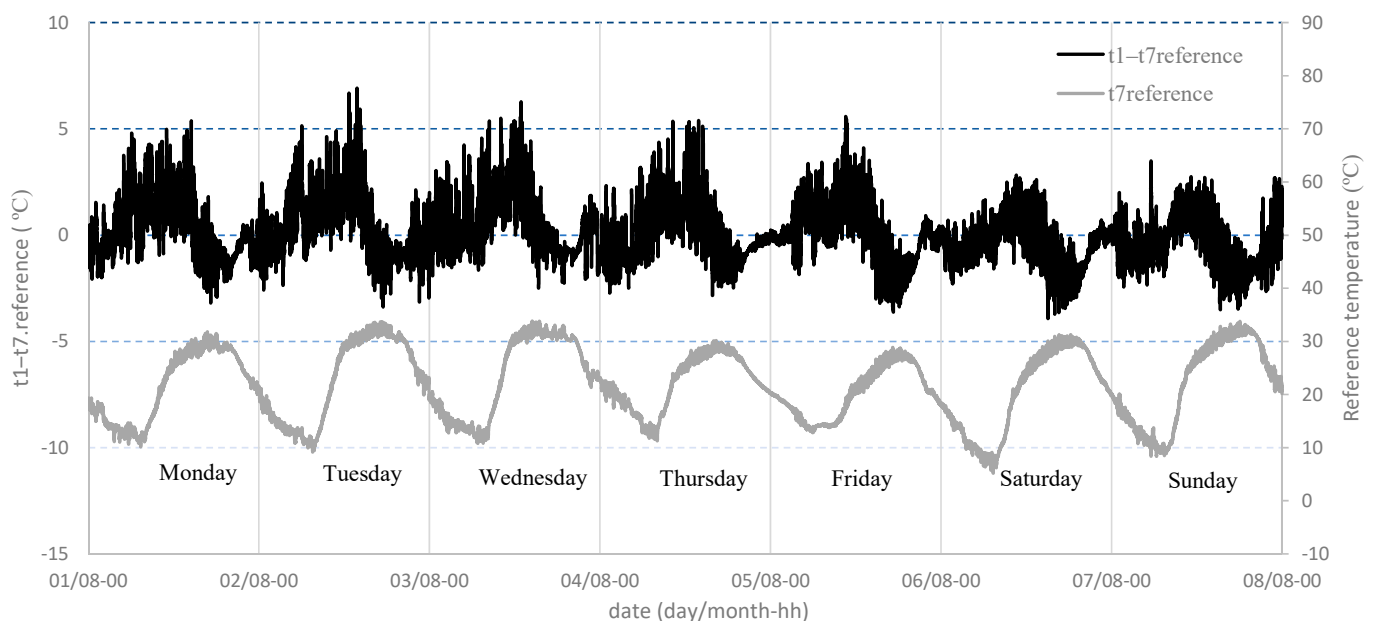

Figure 6. Reference temperature (grey line) and building influence (black line) at pole 1 for a complete week. Data obtained for sunny days with a daily maximum solar irradiance for each of the days of the week ~1000 W/m^2. Working days (Mo–Fr) and weekends (Sa–Su).

Figures 5 and 6 highlight the strong influence of human activity on air temperature measurements at pole 1 (black line) since the reference temperature (grey line) keeps almost stable along each of the weeks. The building influence during the working days is higher than during the weekends—up to 5 °C during working days and up to 2 °C during the weekend in Figure 5. Comparing Figures 5 and 6, it can be seen that the building effect

during working days decreases with the reference temperature, probably due to the nature of the activity performed inside the building; this implies the use of furnaces at high temperatures, with a higher impact when outside is cold.

As a consequence, and in order to perform an analysis as independent as possible from human activity, the later sections and the conclusions of this paper focus on the building impact on air temperature during the weekends and holidays, when there is no activity inside the building.

3.2. Evolution of the Building Influence during the Day at the Pole 1 and Factors of Influence

The evolution of the building influence on air temperature measurements during the day was studied at the position where the highest effect is expected—at pole 1 (1 m). The complete 1-year data set was analyzed in order to find the systematic evolution of the building influence on air temperature measurements. An example of this evolution is represented in Figures 7–10 for two specific totally sunny days, with a maximum solar irradiance of 470 W/m^2. In each of the figures, the progression of one of the additional meteorological quantities measured in this study is also represented. The aim of Figures 7–10 is to determine the meteorological quantity with the highest impact on building influence.
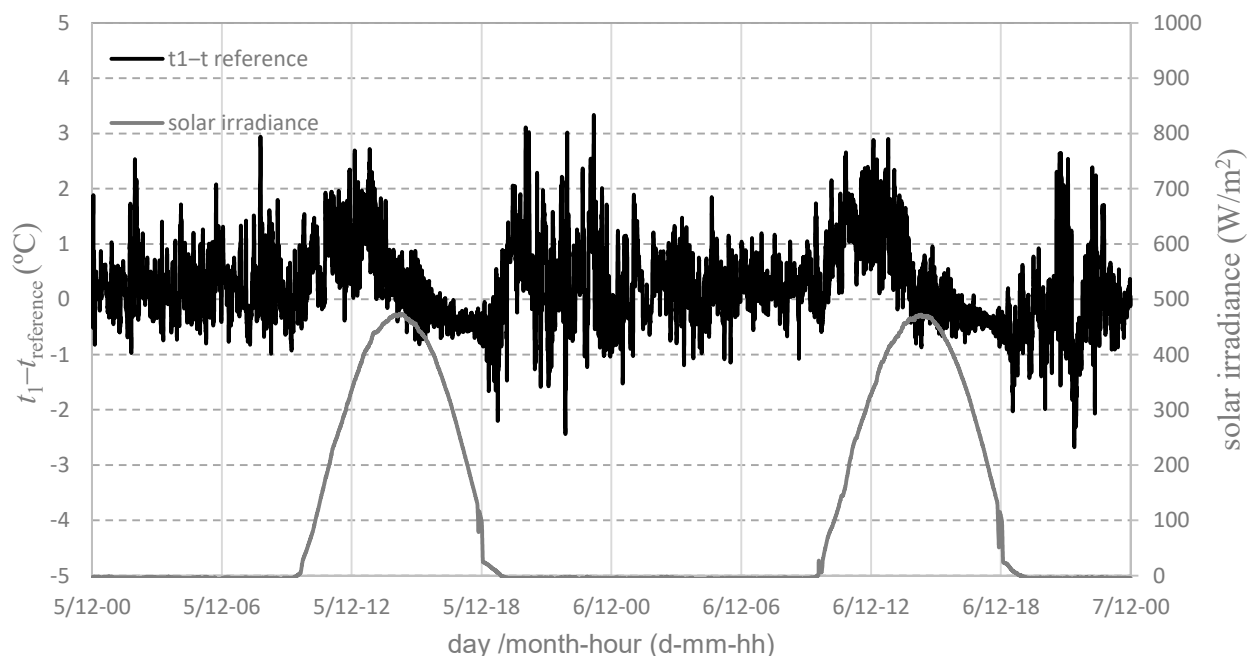

Figure 7. Building effect at pole 1 on sunny days and solar irradiance (5th and 6th of December).

3.2.1. Impact of Solar Irradiance on Building Influence

Figure 7 shows the building influence at pole 1 in combination with solar irradiance. A positive building effect ($\Delta t_1 > 0$) is generated when the solar irradiance increases. Before the solar irradiance reaches its highest value, the building effect decreases to a negligible value, and the building effect evolves to negative values with the decreasing of the solar irradiance in the afternoons. At night, without solar radiation, the building effect tends to recover, little by little, to the zero value. Figure 7 suggests a connection between the building effect at pole 1 and the solar irradiance evolution during the day. This is confirmed in Figure 11, where the building effect variation is displayed for two cloudy days, with maximum solar irradiances of around 750 W/m^2 and 550 W/m^2, respectively. These solar irradiance values are higher than the ones in Figure 7 and, despite this fact, the building influence for sunny days (Figure 7) is higher than for cloudy days (Figure 11). In addition, Figure 11 confirms the correlation between the variation of the building effect at pole 1 and the evolution of the clouds during the day. In Figure 11, the building effect takes a

negligible maximum value for the first day and around +1.8 °C for the second day. The almost negligible positive building effect on the 21st of November is because that day was cloudy during the morning; meanwhile, the almost negligible negative building effect ($\Delta t_1 < 0$) for the 22nd of November is a consequence of the sharp solar irradiance drop in the afternoon due to the clouds. These results support the conclusion that the building effect on cloudy days depends on the evolution of the clouds during the day. These conclusions are supported by the observations during other cloudy days along the year-long lifetime of the experiment.
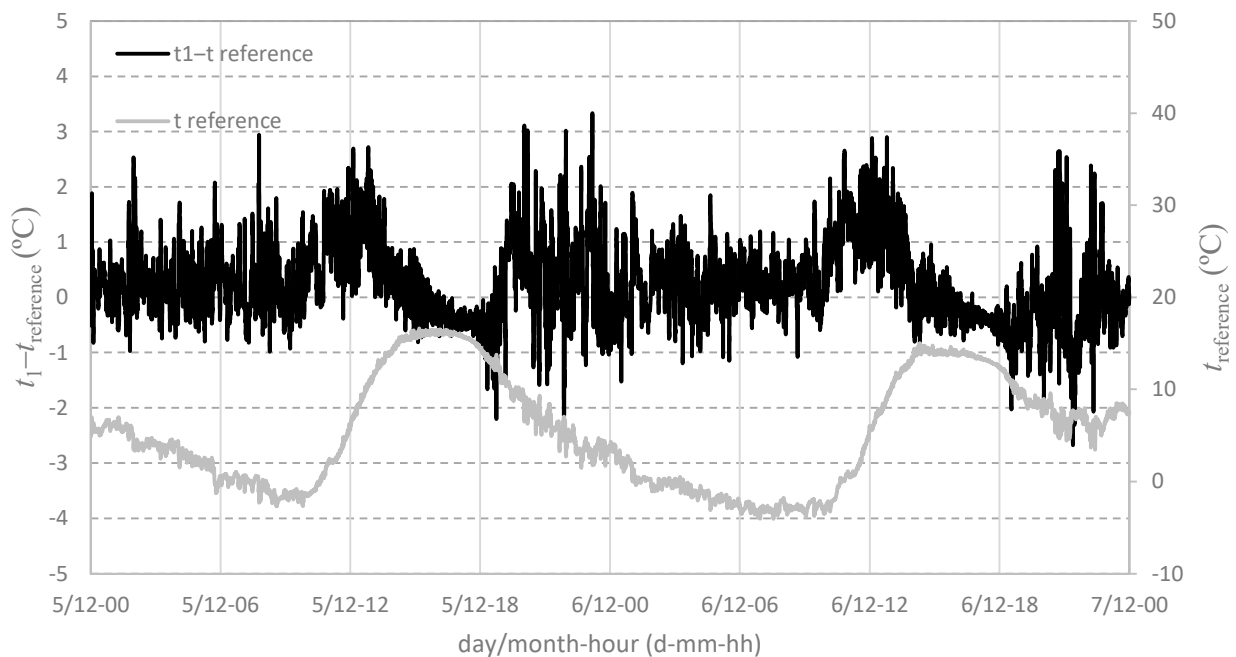
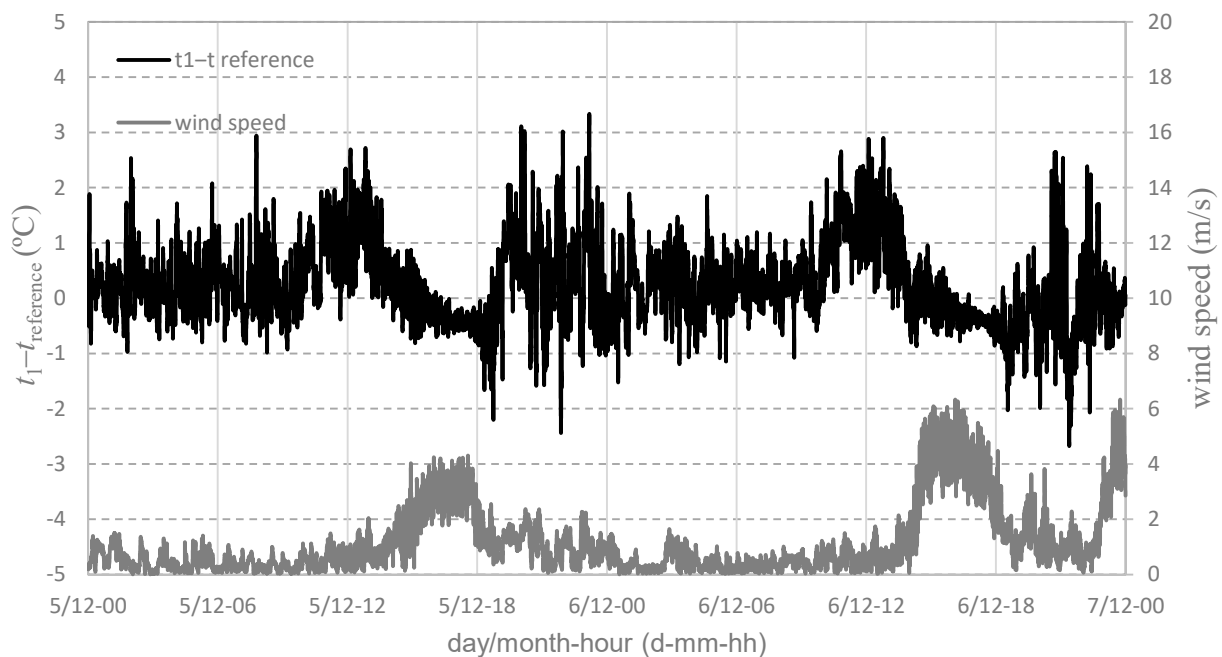**Figure 8.** Building effect at pole 1 on sunny days and air reference temperature (5th and 6th of December).

Figure 9. Building effect at pole 1 on sunny days and wind speed (5th and 6th of December).
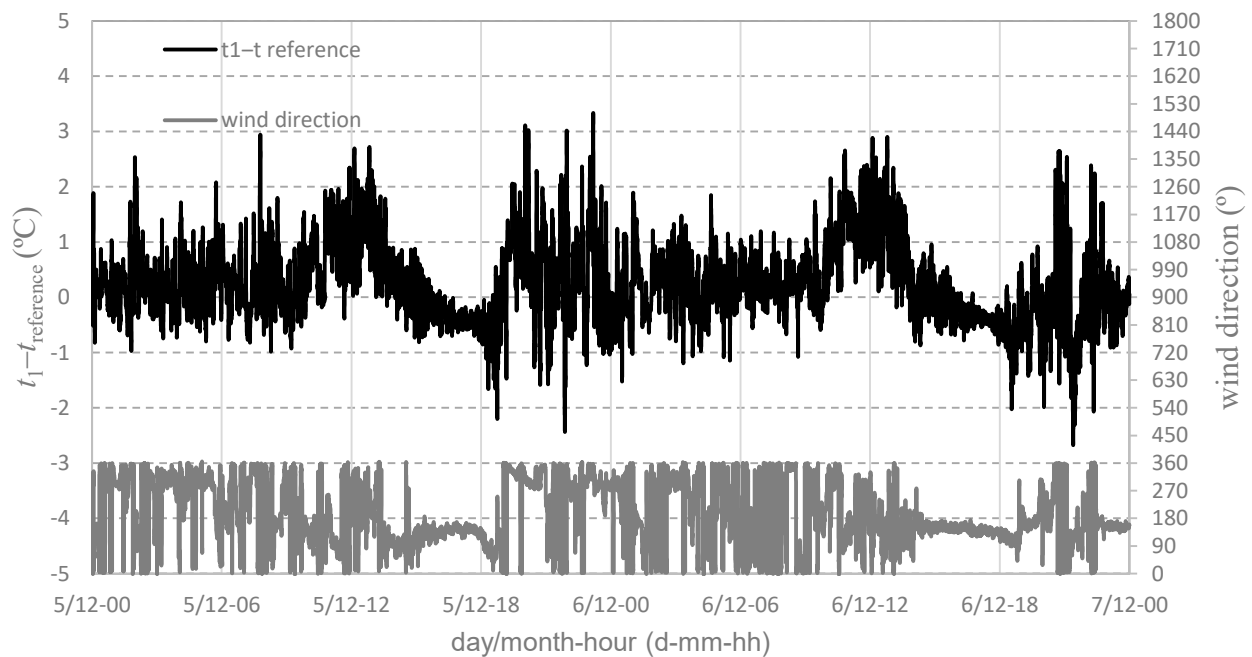
Figure 10. Building effect at pole 1 on sunny days and wind direction (5th and 6th of December).
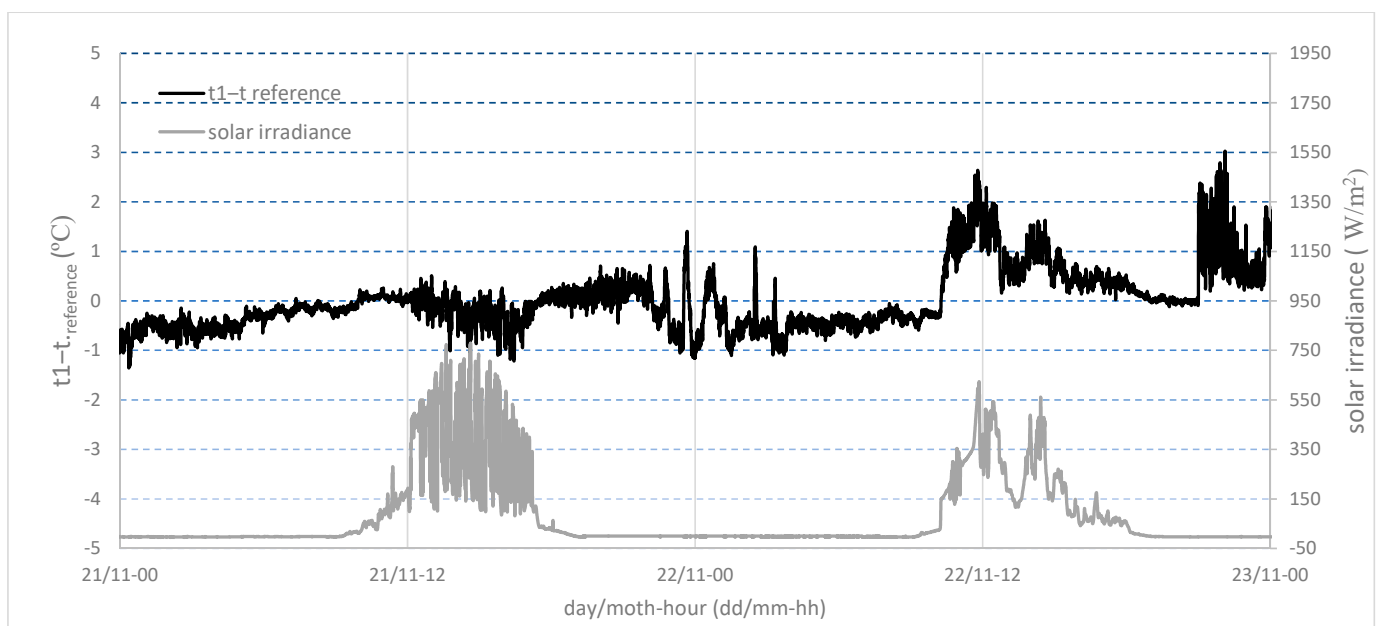

Figure 11. Building effect at pole 1 on cloudy days (21st and 22nd of November).

Then, as a conclusion, the building influence is lower on cloudy days than on sunny days. Because this work is focused on finding the extreme values of the building effect, the following sections concentrate on the building influence for sunny days, with solar irradiance being the main impact factor.

3.2.2. Impact of Daily Maximum Air Temperature on Building Influence

The impact of the daily maximum air reference temperature on building influence could be derived from Figure 8, where the building effect on two different days and with different maximum air reference temperatures: 16.3 °C and 14.5 °C, are represented. The dependency of the building influence value with the reference temperature at pole 7 is not conclusive in Figure 8, where the building effect on two different days and with different

maximum air reference temperatures are represented. The maximum air temperature difference on these two days is not significant enough to assure that the air temperature does not impact on building influence. A further analysis is represented in Figures 12 and 13, where the maximum positive and negative building effects on pole 1 as a function of the daily maximum air reference temperature are represented for totally sunny weekends. These figures suggest that the building influence increases with the daily maximum air reference temperature, but there was one particular day with a low maximum reference temperature (12.7 °C), high solar irradiance (1013 W/m^2), and high building influence on pole 1. This fact, in combination with the conclusions in other research works [21,22], induces to think that the real factor driving the building influence is the solar irradiance instead of the air temperature. The correlation between the daily maximum values of the solar irradiance and the maximum air reference temperature for sunny weekends along the total time of the study is displayed in Figure 14. In this figure, we can see that the correlation between these two quantities is clear for the data of summer and autumn. Discrepancies to this correlation is for the days with maximum air temperature lower than 15 °C and solar irradiance higher than 700 W/m^2. As it is established in [21], these anomalous values could be due to the minimum temperatures happening just before these daily maximum values. If the correlation between the daily maximum values of solar irradiance and air reference temperature had been clearer and more direct, we could have chosen the air reference temperature instead the solar irradiance as the main impacting factor of building influence. But, as this correlation is not so coherent here, this work focuses on studying the impact of solar irradiance on building influence to quantify their maximum values.

Figure 12. Maximum positive building influence at pole 1 (1 m) as a function of maximum air reference temperature for clear weekend days. Black squares are the measured building effect at pole 1 as a function of the corresponding maximum air reference temperature. Dotted line is the interpolation curve.
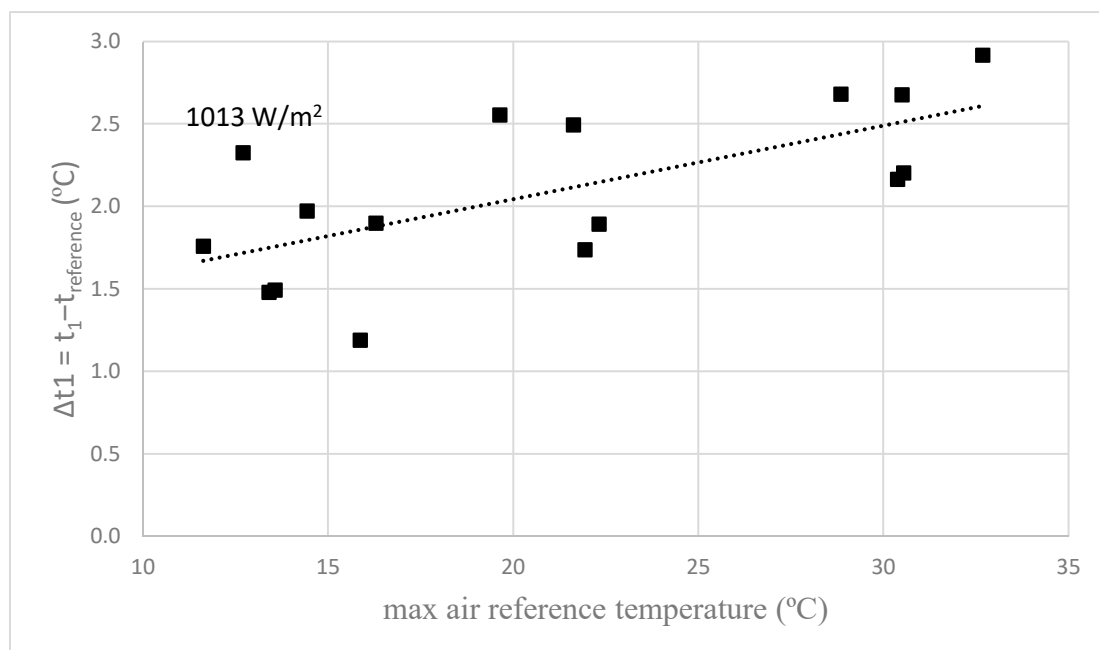
Figure 13. Maximum negative building influence at pole 1 (1 m) as a function of maximum air reference temperature for clear weekend days. Black squares are the measured building effect at pole 1 as a function of the corresponding maximum air reference temperature. Dotted line is the interpolation curve.
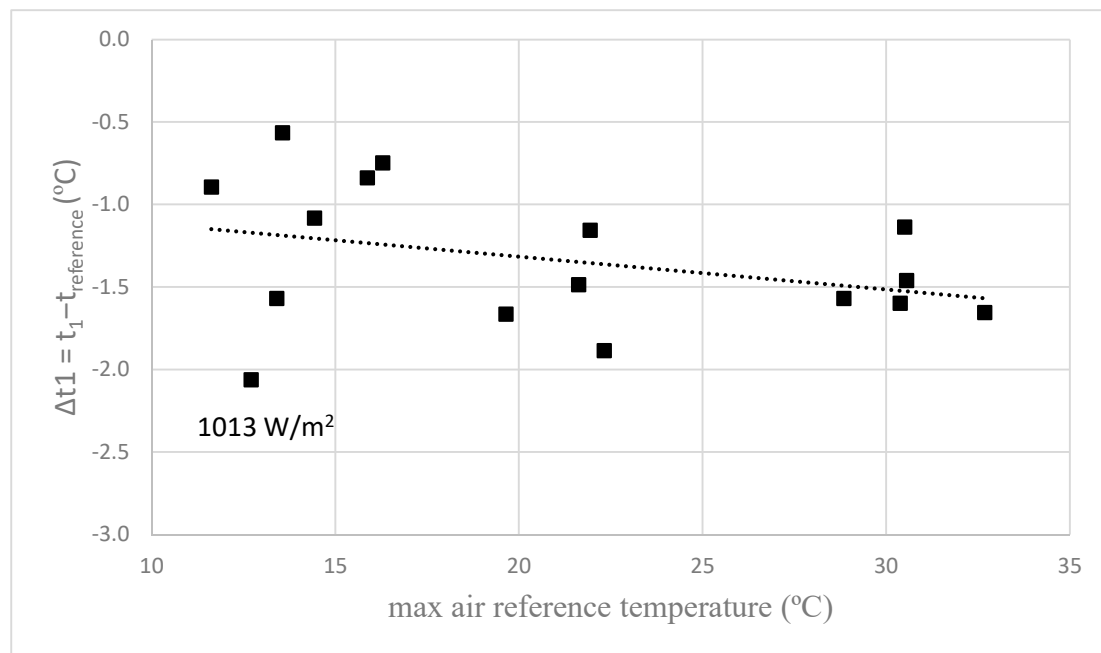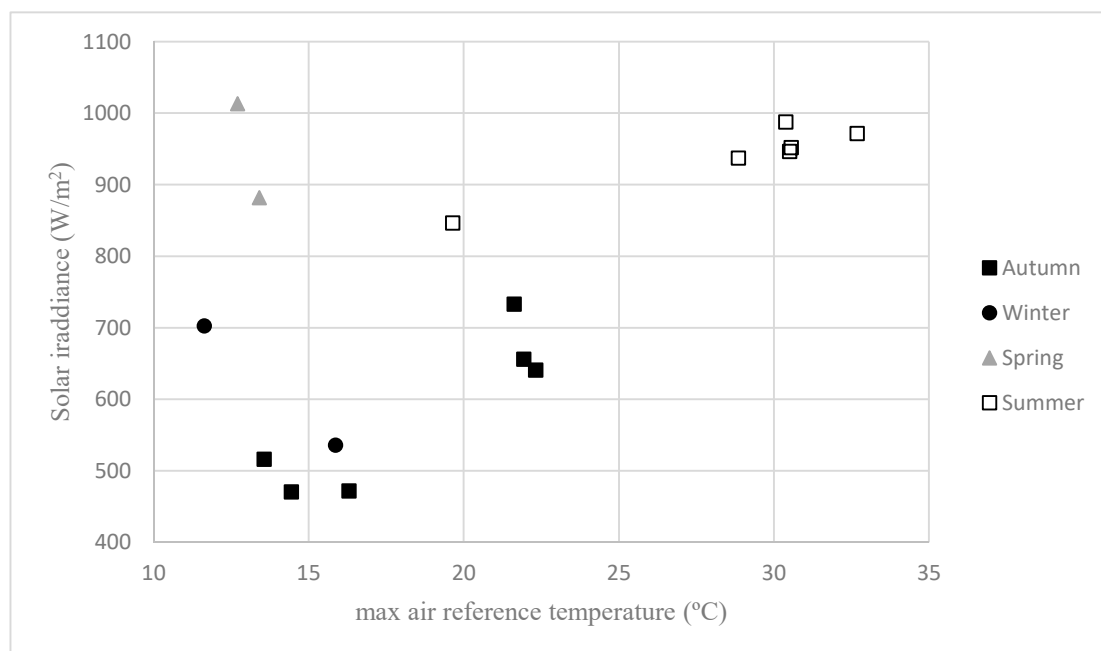

Figure 14. Correlation between the daily maximum values of solar irradiance and reference air temperature for sunny days.

3.2.3. Impact of Wind on Building Influence

Figures 9 and 10 give an indication of the wind impact on building influence. Figure 9 shows the building effect and wind speed; meanwhile, Figure 10 shows the building effect and wind direction for the same sunny days, 5th and 6th of December. These figures show that for wind speeds lower than 2 m/s the air is in turbulent flow, while for higher speeds the air is stratified in a direction parallel to the building (~180°). This behavior

for these two specific days is confirmed in Figure 15 for all of the sunny weekends (when a higher building effect is expected) along the complete time of the experiment (1 year). Figure 15 shows that the experiment site is characterized by low speed wind events. The most frequent ones (75.6%) present wind speeds lower than 2 m/s and in a light turbulent flow but with a dominant component from the NNW to SSE, parallel to the building. Events with wind speed in the ranges (2, 4) m/s, (4, 6) m/s and higher than 6 m/s have the respective frequencies of 20.7%, 3.5%, and 0.14%. All of these events have dominant flow directions parallel to the building and, as consequence, affect all of the thermometers installed in the poles in the same way, in a perpendicular line to the building (Table 1). It can be concluded that, for wind speeds higher than 2 m/s, all of the thermometers are affected in the same way and there is no wind influence on the building effect. For wind speeds lower than 2 m/s, the impact on the building effect can be considered negligible, due to the very low speed value and also due to the majority of the events happen in a direction parallel to the building.
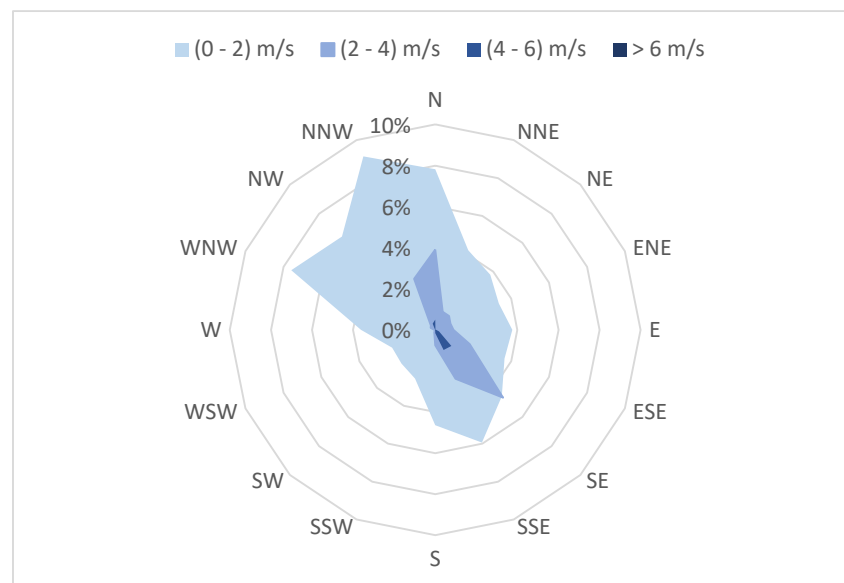

Figure 15. Frequency distribution of wind events at pole 4 and for sunny weekends. Wind measurements were taken every 20 s. N for winds from north to south, E for winds from east to west, W for winds from south to north, and S for winds from west to east.

3.3. Theoretical Determination of the Building Shadow Time on the Poles

In order to check that the negative building effect is a real building effect and it is not due to limited solar radiation blocking by the thermometer shield, a theoretical calculation of the starting shadow time ("sunset") over each thermometer was performed.

The theoretical calculation of the starting building shadow time on the poles was performed via the means of a digital elevation model of the building combined with solar ephemeris, by writing R code and making use of several additional packages: "shadow" [23] "ggmap" [24] "rgdal", "rgeos" and "maptools" [25]. Packages "rgeos" and "rgdal" were used at first to create a digital model of the building of this study and of the poles hosting the temperature sensors. "Maptools" and "solarpos" were used to create a time series of sun positions, calculated each 10 min, within the twelve months of the study (November 2015–December 2016); "shadow" and "shadow Height", fed by results from "solarpos" and the digital model of the building, were then used to compute the heights of the shadow cast by the building at the locations of the sensors, at each time step considered. By comparing these heights to the heights of the sensors, information about whether the sensor is in the shadow of the building or not, and at what time it enters or exits the shadow, is retrieved. Finally, "ggmap" was used to retrieve the image area from Google Maps and plot buildings and shadows on top of it.

The program code was able to calculate, with a time resolution of 10 min, the time when the building shadow reached specific heights of each pole and, hence, the thermometer sited in each of the poles. By comparing this value with the height of the poles (2.0 m), a timetable of "sunsets" for each thermometer was compiled for the whole duration of the experiment. A height of 2 m was chosen to be sure the thermometers and the radiation shields (1.5 m) were completely under the shadow of the building for the calculated times.

The theoretical calculations of these "sunset" shadow times on the thermometers were combined with the complete data set of building influences on the sunny weekends. The behavior is observed in Figure 16, where there are representations of the building effect at different distances from the building as a function of time. Figure 16 represents a specific day, as an example, but the same behavior was observed for the rest of the days under analysis. In order to have a better vision of the time when the starting sunset shadow happened and when the minimum building effect happened, the raw data were integrated with an integration time of 20 min. From Figure 16, we can conclude that the negative building effect ($t_i < t_{reference}$) is not a direct and instant consequence of the sunset shadow of the building over the corresponding thermometer. This sunset shadow time (the time at which the building shadow just covers the thermometer) is always earlier than the minimum building influence. The negative building influence is due to a combination of factors, one of them being the lack of direct solar radiation on the field surrounding each of the poles. In this situation, for a period of time, there is a release of the heat stored in the ground and in the building, collected during the sun exposure along the rest of the day. With time, these stored heats are negligible and then the maximum negative building effect is produced.
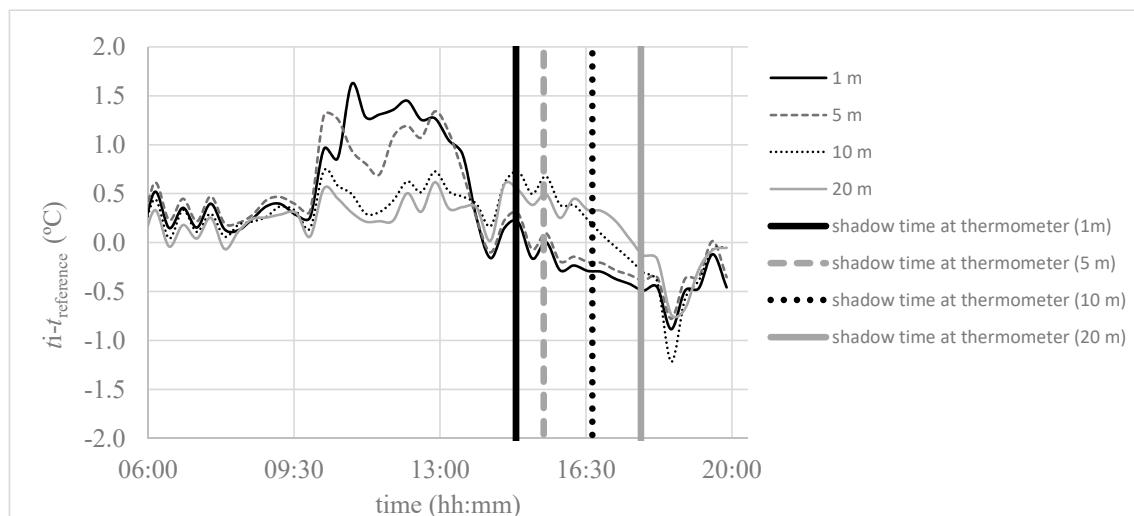

Figure 16. Building influence at different distances from the building (1 m, 5 m, 10 m, and 20 m). The starting times (wider lines) when the thermometers, at each of the poles, are covered by the shadow of the building are also included. For this specific day, shadow time for thermometer at 1 m: 14:50, shadow time for thermometer at 5 m: 15:30, shadow time for thermometer at 10 m: 16:40, and shadow time for thermometer at 20 m: 17:50.

3.4. Quantification of the Building Influence on Air Temperature

3.4.1. Optimal Integration Time Interval

Before approaching the quantification of the building influence on air temperature measurements, a study of the most appropriate data management was performed. The temperature measurements were averaged at different time intervals to obtain the most realistic description of the building influence evolution along the day. The most optimal integration time was decided by reaching a compromise between the following: (i) Keeping as much information as possible and not reducing the maximum building effect; (ii) Reduc-

ing noises and peaks not related to real changes in temperature. Figure 17 displays the effect of averaging the raw data at several time intervals. If the averaging time interval is long, the noise will be removed; but, there is the risk that some real effects on air temperature are also reduced or eliminated. On the contrary, if this time period is very short, the removal of the noises and peaks would not be enough for the appropriate analysis. Based on the information provided in Figure 17, the averaging time of 5 min reaches the appropriate compromise between the removal of the measurements noise and keeping enough information at the same time. Despite this fact, later in this paper, the quantification of the building influence on air temperature measurements is performed for other integration times.
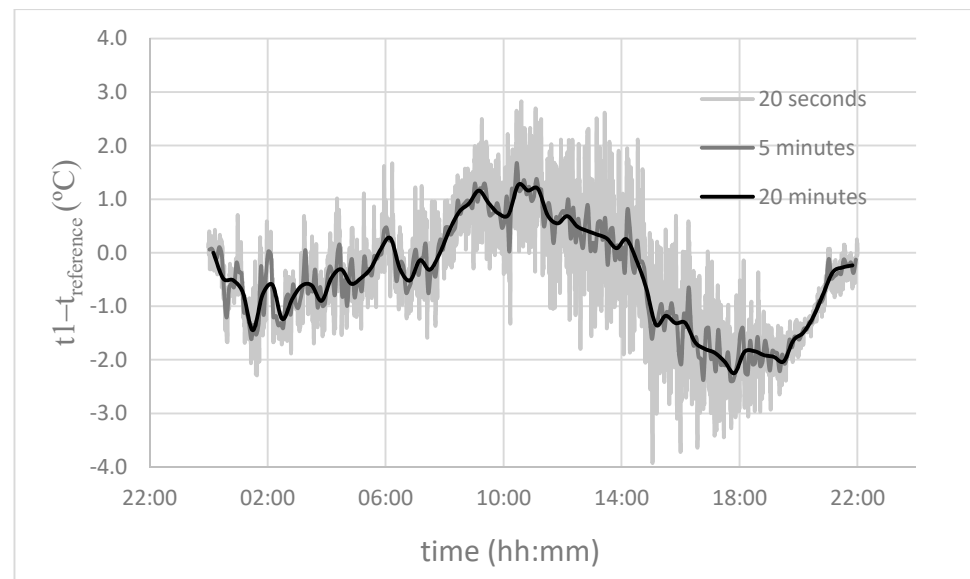

Figure 17. Evolution of the building influence on air temperature measurements at pole 1 at different integration times.

3.4.2. Solar Irradiance and Building Influence at All Poles

As it was described before, in Section 3.2, the building has an effect on the air temperature. Due to the orientation of the building, in the mornings the building acts as a heat source, increasing the temperature of the surrounding area regarding the reference temperature (positive building effect). This fact is mainly due to the solar irradiance impact on the building: on one hand, it is reflected by the building walls; on the other hand, it is absorbed by the walls and released little by little into the environment. In the afternoons, the building shadows the ground surrounding the thermometers and the heat released by this ground decreases gradually with time and, as a consequence, the temperature at the shadowed positions also decreases regarding the reference air temperature (negative building effect). The surface under the building shadow increases with time and, hence, the building has an impact at larger distances. Then, the building influence on air temperature measurements is positive in the mornings and negative in the afternoons. In the positive building effect the air temperature decreases with the distance to the building; meanwhile, in the negative building effect the air temperature increases with the distance to the building. As we already stated, the human activity inside the building and the solar irradiance are the main impacting factors on building influence; so, in order to quantify the maximum building effect (independently from human activity inside the building), the data considered in this analysis are the ones obtained on sunny weekends from November 2015 to November 2016.

For these sunny weekends, the maximum values of the building effect were determined from repetitive events happening during each of the days and with stable temperature conditions for more than 1.5 h. This duration was chosen with the aim of removing

punctual issues or noisy episodes from the analysis and to be sure that the analysis was based on a real and systematic building effect.

Figures 18 and 19 show the relationship between the building influence at different distances from the building and the solar irradiance. The two building influences increase with solar irradiance, mainly for the closest thermometer to the building (pole 1, 1 m).
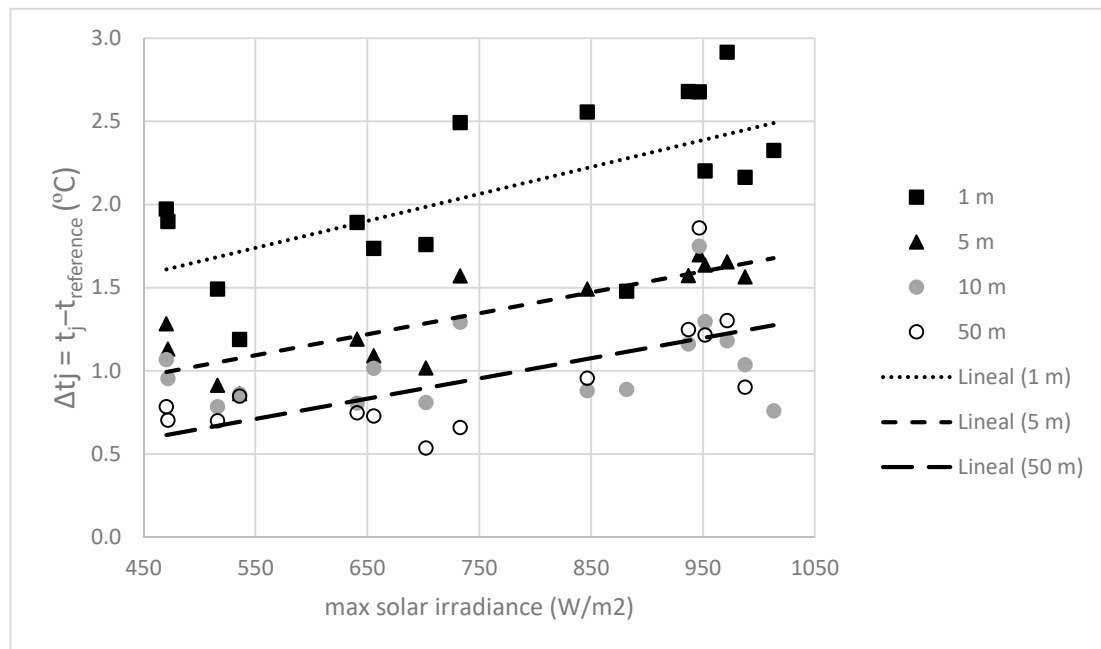

Figure 18. Maximum positive building effect as a function of maximum sun radiation.
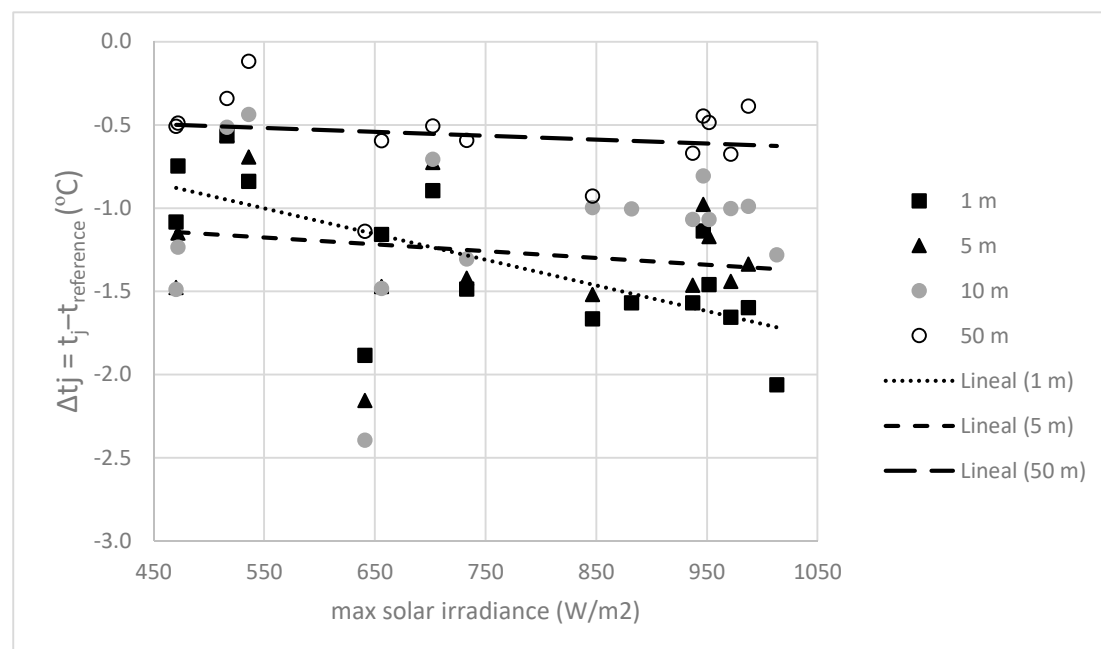

Figure 19. Maximum negative building effect as a function of maximum sun radiation.

Based on the information provided by the Figures 18 and 19, a range of solar irradiance, (850, 1000) W/m^2 was chose for the determination of the extreme building effects.

3.4.3. Maximum Values for Building Influence

The maximum building influences for the solar irradiance range $(850, 1000)$ W/m^2 are represented in Figures 20 and 21. These values are not negligible and take values up to 2.0 °C at a distance of 1 m from the building. These figures show the building effect decreases with the distance to the building and it trends towards a zero value for distances higher than 50 m. This long distance for the building effect mitigation could be related to the large width of the building (200 m). The inclusion of thermometers at longer distances larger than 50 m from the building would have added important information to this study.
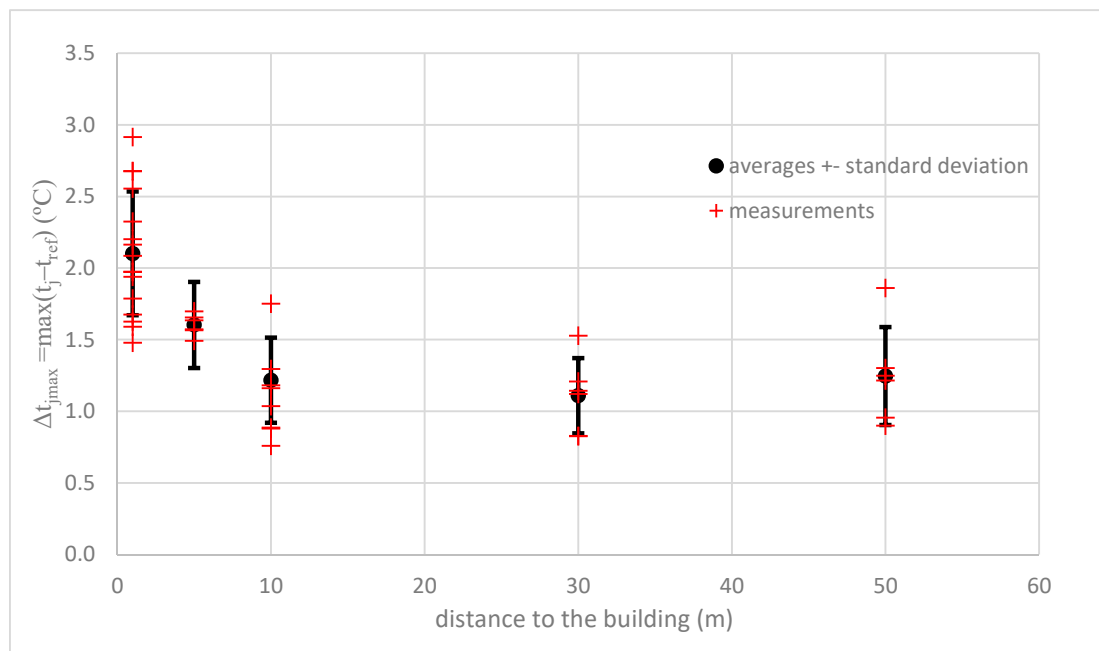

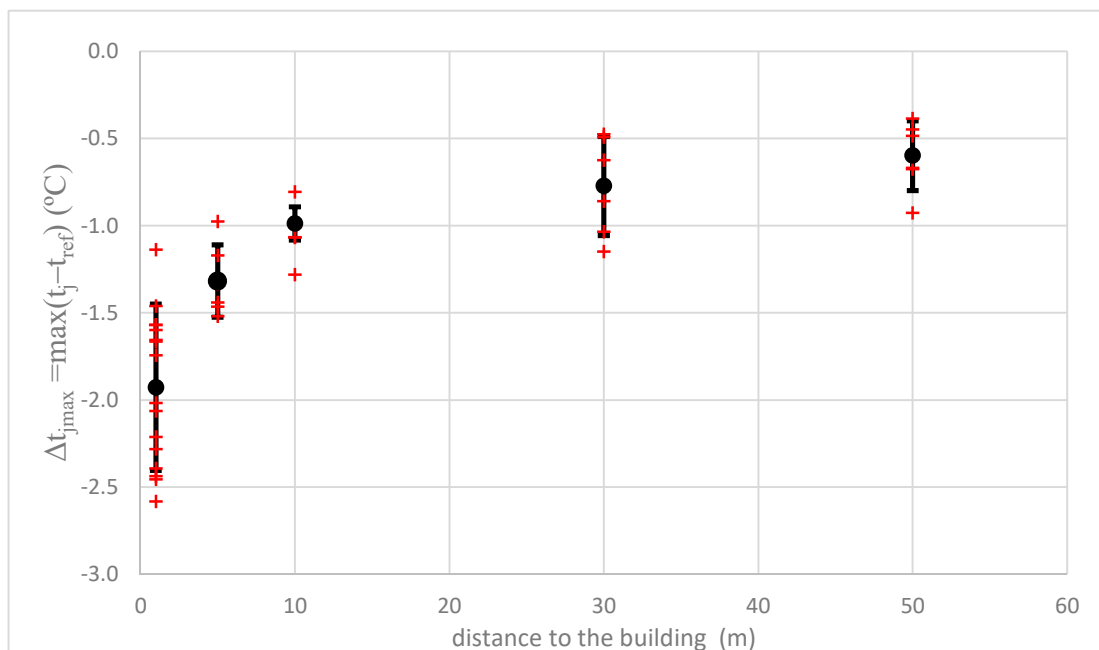**Figure 20.** Maximum positive building effect for solar irradiance in the range $(850, 1000)$ W/m^2.

Figure 21. Maximum negative building effect for solar irradiance in the range $(850, 1000)$ W/m^2.

3.5. Uncertainties

The building influence at different distances from the building is calculated using Equation (4) and with more detail from Equation (5).

$$\Delta t = t_i - t_{reference} \tag{4}$$

$$\Delta t = (t_i + \delta t_{i,\,calibration} + \delta t_{i,\,drift} + \delta t_{i,\,reading\,system}) - (t_{ref} + \delta t_{ref,\,calibration} + \delta t_{ref,\,drift} + \delta t_{ref,\,reading\,system}) + \delta t_{repeatability} \tag{5}$$

To calculate the building effect associated uncertainty, the law of propagation of uncertainties [3] should be applied to (5) resulting in the following:

$$u^2(\Delta t) = u^2\left(t_i - t_{ref}\right) + 2 \cdot u^2(\delta t_{calibration}) + 2 \cdot u^2\left(\delta t_{drift}\right) + 2 \cdot u^2\left(\delta t_{reading\,system}\right) + u^2\left(\delta t_{repeatability}\right). \tag{6}$$

The description and quantification of the different uncertainty sources are included in Table 3.

The procedure to estimate each uncertainty component is evaluated:

- Uncertainty contribution due to the standard deviation of the differences:

This uncertainty component was evaluated using the standard deviation of the building effects obtained during sunny days with a sun radiation in the range 850–1000 W/m^2, where the building effects are stronger.

- Uncertainty contribution due to the calibration of the thermometers:

The uncertainty component due to the calibration of the thermometers is the value of the expanded calibration uncertainty value divided by the coverage factor. The calibration of the thermometers was performed just before and after the field experiment, as described in point 2.1. In both cases, the expanded calibration uncertainty was 0.01 °C (k = 2).

- Uncertainty contribution due to the drift of the thermometers:

This uncertainty component was evaluated using the means of the resistance value of each thermometer at the triple point of water (0.01 °C), as it is described in point 2.1. The value of the drift of the thermometers is 0.02 °C.

- Uncertainty contribution due to the reading system:

This uncertainty component was evaluated using the combination of the datalogger calibration and resolution, with a value of 0.05 °C (k = 2):

$$u^2\left(\delta t_{reading\,syst}\right) = u^2\left(\delta t_{reading\,syst-calibration}\right) + u^2\left(\delta t_{reading\,syst-resolution}\right). \tag{7}$$

- Uncertainty contribution due to the repeatability of the thermometers:

This uncertainty component was evaluated by analyzing the different behavior of the thermometers under the same field exposure conditions, thereby obtaining a value of 0.1 °C [9].

Table 3. Uncertainty evaluation for building influence.

Description	Quantity	Method of Estimation	Probability Distribution	Sensitivity Coefficient	Uncertainty Contribution, 1 m	Uncertainty Contribution, 5 m	Uncertainty Contribution, 10 m	Uncertainty Contribution, 30 m	Uncertainty Contribution, 50 m	Uncertainty Contribution, 100 m
Medium diference temperature:	$t_i - t_{ref}$	Standard deviation of the differences	normal	1	0.300	0.165	0.224	0.145	0.217	0.000
Reference thermometer calibration	$\delta t_{ref\text{-}cal}$	Calibration uncertainty ($k = 2$)	normal	2	0.050	0.050	0.050	0.050	0.050	0.050
Reference thermometer drift	$\delta t_{ref\text{-}drift}$	Difference between the initial and final calibration	rectangular	$\sqrt{3}$	0.006	0.006	0.006	0.006	0.006	0.006
Pole i thermometer calibration	$\delta t_{i\text{-}cal}$	Calibration uncertainty ($k = 2$)	normal	2	0.050	0.050	0.050	0.050	0.050	0.000
Pole i thermometer drift	$\delta t_{i\text{-}drift}$	Difference between the initial and final calibration	rectangular	$\sqrt{3}$	0.006	0.006	0.006	0.006	0.006	0.000
Reading system	δt_{system}	Resolution+Calibration	normal	1	0.024	0.024	0.024	0.024	0.024	0.024
Repeatability	$\delta t_{repeatability}$	Difference of the thermometers readings at the same external conditions [9]	normal	1	0.100	0.100	0.100	0.100	0.100	0.100
Combined standard uncertainty, in °C=					0.33	0.21	0.26	0.19	0.25	0.11
Expanded uncertainty ($k = 2$), in °C=					0.65	0.41	0.51	0.38	0.50	0.23

3.6. Building Influence with Other Average Intervals

In order to analyze the dependence of the building influence against the data average time interval, the same analysis previously described was performed for different time intervals, with the conclusions displayed in Figure 22. As was expected, the building effect decreases against time averages since the maximum values smoothen against time average. Another conclusion is that the building effects are not a consequence of punctual extreme values from noises or aleatory effects.
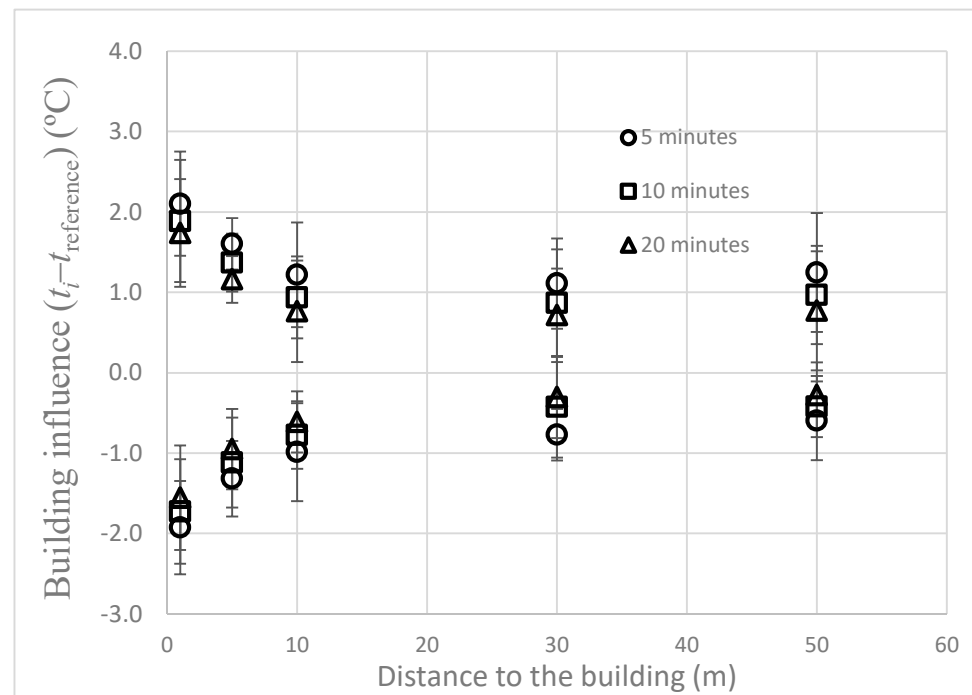

Figure 22. Building effect at different average times: ◯ Integration time: 5 min. ☐ Integration time: 10 min. Δ Integration time: 20 min.

Using the 20 min averaging data, the functions describing the positive and negative building effect $y(d)$ were calculated in the form

$$y(d) = t(d) - t_{ref} = a - b \cdot \ln d \tag{8}$$

where d is the distance to the building and a and b are the coefficients calculated via fitting to the data. These functions were calculated using the least squares method [26], minimizing the standard deviation of the residuals ($s = \sqrt{\frac{\left(\sum_{i=1}^{n} q_j - \bar{q}\right)^2}{n-1}}$). These functions and data are displayed in Figure 23, where the building effect functions present residuals lower than the uncertainty of the measurements, meaning the goodness of the function's fit to the corresponding measured points). Table 4 provides the two building functions, with the corresponding residual's standard deviation. The uncertainties of the interpolation coefficients, a and b, where calculated using the classical Ordinary Least Squares theory [26]. Table 5 includes these uncertainty values.
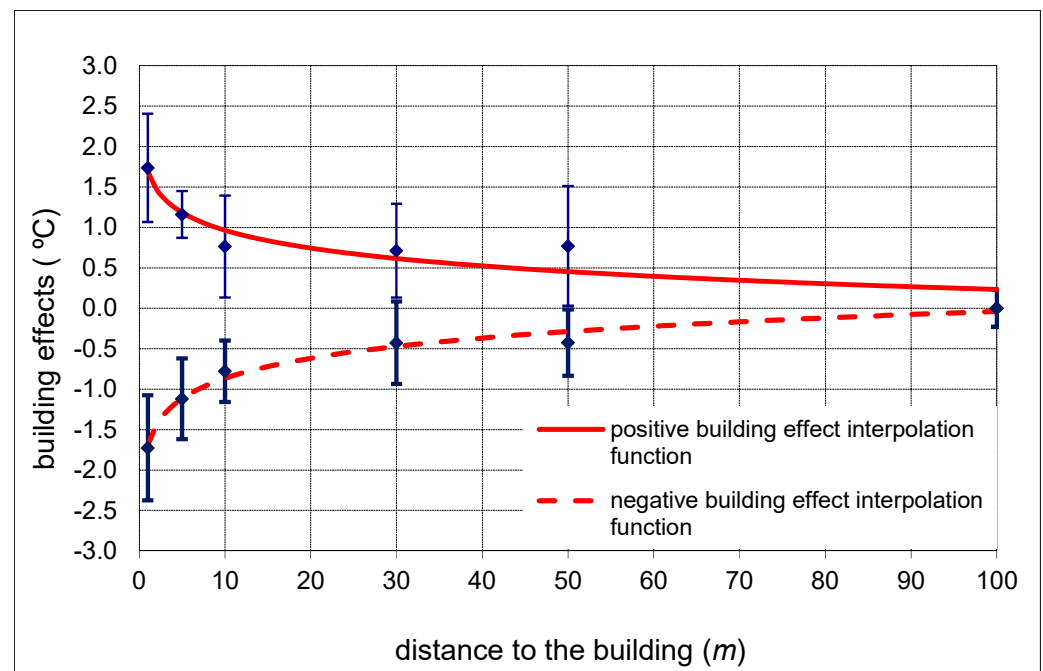
Figure 23. Positive and negative building effect functions determined using their fitting to the corresponding 20 min averaged data (blue points), Its corresponding expanded uncertainty ($k = 2$) is also represented.

Table 4. Positive and negative building effects functions, standard deviation of the residuals, and R^2.

	Building Effect Function	$s=\sqrt{\dfrac{\left(\sum_{i=1}^{n} q_j - \overline{q}\right)^2}{n-1}}$	$\mathbf{R^2}$
Positive building effect	$f_p(d) = 1.696 - 0.317 \cdot \ln d$	0.20 °C	0.87
Negative building effect	$f_n(d) = -1.693 + 0.359 \cdot \ln d$	0.08 °C	0.98

Table 5. Uncertainties of the interpolation function's coefficients.

	U(a), ($k = 2$)	**U(b), ($k = 2$)**
Positive building effect	0.185	0.061
Negative building effect	0.070	0.023

The uncertainties of the building effect at different points, displayed in Figure 23, were calculated following the procedure described in Section 3.5. The uncertainty of the interpolation functions was calculated using the propagation of the uncertainties of the building effects at the discrete points [27,28], keeping in mind that the interpolation functions were calculated via the linear least-squares method (non-Lagrangian interpolation equations). The uncertainty of an interpolation function can be calculated easily when the interpolation function can be written in the form:

$$\hat{y}(x) = \sum_{i=1}^{N} y_i \cdot f_i(x,\ x_i,\ \dots x_N). \tag{9}$$

The expression for the uncertainty associated with the interpolation curve is derived by applying the law of propagation of uncertainties [3] to (9).

$$u^2(\hat{y}(x)) = \sum_{i=1}^{N} f_i^2(x,\ x_1, \dots x_N) \cdot u^2(y_i) \tag{10}$$

For the building effect the interpolation functions are

$$y(d) = t(d) - t_{ref} = a - b \cdot \ln d = \sum_{i=1}^{N} y_i \cdot (f_{1i} + f_{2i} \cdot Ln(d)). \tag{11}$$

And, the corresponding uncertainty is

$$u^2(y(d)) = \sum_{i=1}^{N} \left(f_{1i}^2 + f_{2i}^2 \cdot Ln^2(d) \right) \cdot u^2(y_i) + s_{residuals}^2. \tag{12}$$

Figure 24 shows the expanded uncertainties for building effects at discrete points and for the two interpolation functions included in Table 4.
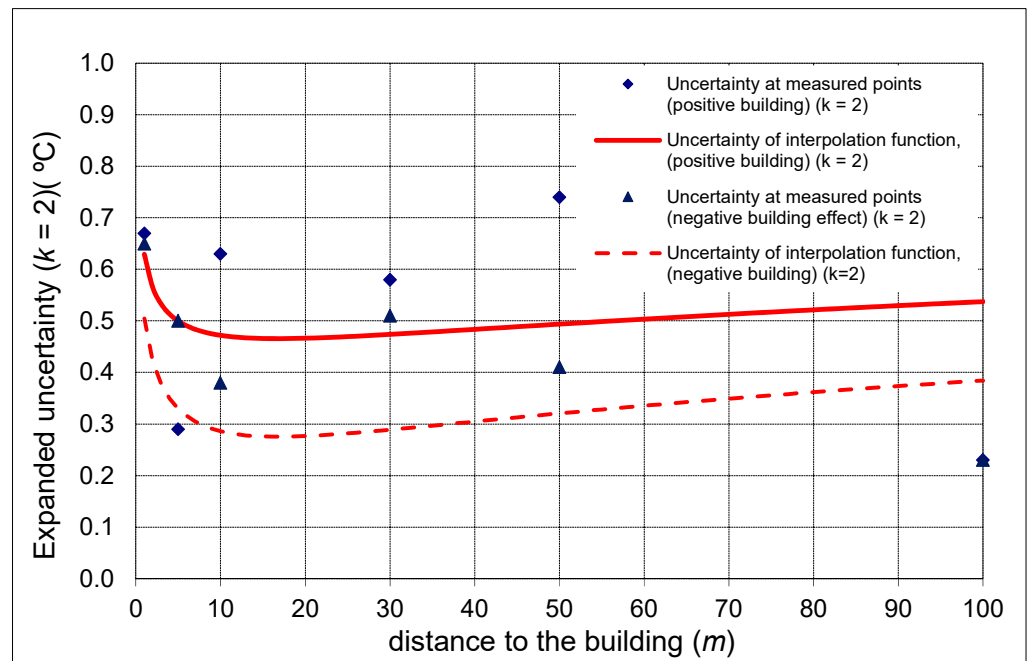

Figure 24. Expanded uncertainties (k = 2) of the building effects at the different discrete points and the expanded uncertainties (k = 2) of the building effect interpolation functions.

4. Conclusions

In this paper the study of the building influence on air temperature measurements has been examined in a field experiment. An extensive search for the appropriate location was performed aiming at Class 1 [1] air temperature measurements. The selected place is a flat area bigger than 40,000 m^2, with a 6 m high and 200 m wide building. No other obstacles or shadows exist in the area. Fit-for-purpose instrumentation was calibrated and characterized with the objective of obtaining measurements following metrological principles, giving, as a consequence, robustness to this paper's conclusions. All of the instrumentation was deployed perpendicularly to the building and at different distances, providing a radial air temperature measurement distribution.

The building influence was evaluated using a one-year-lasting field experiment and its quantification was performed from observed repetitive and systematic events across different days and with a duration longer than 1.5 h. With these considerations in mind, the inclusion of punctual or aleatory phenomena in the analysis was avoided.

The human activity inside the building has a clear impact on the building influence on air temperature measurements. This conclusion is in line with [12], where an increase in anthropogenic heat emission corresponds to an increase in building influence. In this study and in order to remove as much as possible the human impact, only the weekends' data (from the one-year raw data) were considered for the analysis.

This paper also shows the strong dependence of the building influence with solar irradiance as well as with the relative orientation of the building and thermometer, as is also highlighted in [12]. The building influence on air temperature is firmly linked to the evolution of clouds on cloudy days and it is always lower than on sunny days. Cloud cover reduces the building influence on air temperature measurements, as is also stated in [12,15]; the building influence, for sunny days, increases with the maximum daily solar irradiance value, as is also observed in [10].

As the aim of this work was to quantify the extreme building effect, some criteria were followed in order to select the appropriate data set from the one-year raw data. The data from sunny weekends were considered in the analysis. In addition, the optimal integration time was analyzed: 5 min interval. From the examination of this data set, two building effects were detected: one of them happens in the mornings and it consists of an increase in air temperature with proximity to the building (positive building effect). The other one happens in the afternoons and it consists of the decrease in air temperature with proximity to the building (negative building effect). In order to check that there is not any link between the building shadow over the thermometers and the negative building effect, a theoretical calculation of the time when the building shadow reaches each of the thermometer was performed. No direct and instant relation between the negative building effects and the building shadow over the thermometers was found. The decrease in temperature in areas covered by the building shadow was due to a reduction in the radiative effect of surrounding surfaces instead of a malfunction in the system thermometer + shield.

A similar building influence evolution is observed in [10], but it is delayed and lower in value regarding the evolution observed in this work. These differences are due to the fact that the buildings in [10] are smaller than here, meaning the shadow influence in [10] on the ground is very much reduced. The solar exposure of the surfaces (ground and building facade) surrounding the thermometers in both experiments is very different, implying delayed radiative behaviors of these surfaces along the day and, as a conclusion, delayed building effects. In addition to this, the orientation of the buildings is different in both experiments, generating differences in their effects on air temperature measurements. The building facade in [10] is mainly oriented to the north; meanwhile, the building facade involved in this research work is mainly oriented to the east. This means the sun impact on the building facade is more intense and, hence, more building radiative heat is generated in this work than in [10]. The relative orientation between the building and the thermometers determines the quantitative value of the building influence on air temperature measurements and also the evolution of this influence along the day and night.

The establishment of the relation between wind and building effects was not possible in this work due to the special characteristics of this experiment site, where the predominant wind was parallel to the building and, hence, it affected all thermometers in the same way. The impact of wind on building influence studied in previous works [10,12–16], together with the particular relation between the building and the winds described in the present work, allow us to conclude that the impact of wind on the building effect strongly depends on the relative orientation of the building, thermometers, and the dominant wind component in the area under study. This last fact agrees with the conclusions in [15], where the difference between two data climate series in different places is affected by wind direction, mainly for sunny days.

The building influence increases with solar irradiance, making it the strongest impact factor. This relation between building effect and solar irradiance is in line with the conclusions of [10] and other works studying the urban climate [12]. In this research, and in order to find the extreme values of the building effect, a quantification was performed via the selection of an appropriate data set from raw data collected during a one-year experiment: sunny weekends and with a daily maximum solar irradiance in the range 850–1000 W/m^2.

Under these conditions, the positive building effect takes a maximum value of 2 °C at 1 m, decreasing to 1 °C at 10 m, and then stabilizing up to 50 m. The negative building effect

takes a maximum value of $-2\,^{\circ}\mathrm{C}$ at 1 m from the building, it strongly decreases to $1\,^{\circ}\mathrm{C}$ at 10 m, and then decreases smoothly to $0.5\,^{\circ}\mathrm{C}$ at 50 m from the building. Measurements at distances between 50 m and 100 m would have provided valuable information for the determination of building effects at distances greater than 50 m.

The influence of the building effect at 50 m is also observed in [10], although at a lower degree due to a smaller building being included as the influence factor and also due to the mean influence being investigated instead the maximum influence.

The expanded uncertainties associated with all of these values was calculated as having values lower than $0.65\,^{\circ}\mathrm{C}$ ($k = 2$).

The field experiment developed in this research work supports the recommendation that air temperature measurements for reference climate studies should be taken at distances over 100 m from buildings, which is in line with [1,10]. For climate reference stations, the evaluation of studies about the siting influence is recommended. In addition, the development of future studies using buildings at different orientations is recommended, since it is suspected that the relative orientation of the building to the thermometer has a definitive influence on the building effect values.

This work, along with the companion road experiment described in [9], can also constitute a first step towards a more comprehensive experimental description of the complex phenomenon known as "Urban Heat Islands". While some studies report that the influence of urbanization on near-surface temperature measurements is substantial [29], it is difficult to discriminate between different contributing factors that add up to create the island. Models [30–32] can help, but dedicated experiments are needed to validate model computations.

Author Contributions: Conceptualization and methodology: G.C., A.M. and C.G.I.; software: G.C. and A.M.; validation: G.C. and C.G.I.; formal analysis, C.G.I.; investigation, G.C. and C.G.I.; resources, A.M.; data curation, C.G.I.; writing—original draft preparation, C.G.I.; writing—review and editing, G.C. and A.M.; visualization, S.H.; supervision, C.G.I.; project administration, A.M.; funding acquisition, A.M. All authors have read and agreed to the published version of the manuscript.

Data Availability Statement: The data presented in this study are available on request from the corresponding author.

Conflicts of Interest: The authors declare no conflict of interest.

References

1. WMO-No. 8 WMO Guide to Meteorological Instruments and Methods of Observations, Part I, Chapter I, Annex 1D. 2021 Edition. Available online: https://library.wmo.int/idurl/4/68695 (accessed on 25 January 2024).
2. International Vocabulary of Metrology—Basic and General Concepts and Associated Terms. VIM 3rd Edition. JCGM 200:2012 (JCGM 200:2008 with Minor Corrections). 2012. Available online: http://www.bipm.org/utils/common/documents/jcgm/JCGM_200_2012.pdf (accessed on 25 January 2024).
3. Evaluation of Measurement Data—Guide to the Expression of Uncertainty in Measurement, JCGM 100:2008. Available online: http://www.bipm.org/utils/common/documents/jcgm/JCGM_100_2008_E.pdf (accessed on 25 January 2024).
4. Guo, J.; Guan, Y.; Shen, X.; Guo, J.; Tang, Z.; Tian, D.; Xue, Z.; Chen, T.; Mao, J.; You, Y. Experiments and Simulations of Sitting Classification for Wind and Temperature Observation. Available online: https://library.wmo.int/records/item/53114-wmo-technical-conference-on-meteorological-and-environmental-instruments-and-methods-of-observation#.XiroCTJKiUk (accessed on 25 January 2024).
5. Kinoshita, N. An Evaluation Method of the Effect of Observation Environment on Air Temperature Measurement. *Bound. Layer Meteorol.* **2014**, *152*, 91–105. [CrossRef]
6. Kumamoto, M.; Otsuka, M.; Sakai, T.; Hamagami, T.; Kawamura, H.; Aoshima, T.; Fujibe, F. Field Experiment on the Effects of a Nearby Asphalt Road on Temperature Measurement. *SOLA* **2013**, *9*, 56–59. [CrossRef]

7. Umehara, K.; Hosomichi, A.; Kawano, S.; Mour, H. Field experiments to determine the effect of boundary fences on temperature Observation. In Proceedings of the WMO/CIMO/TECO-2016 SESSION 3—Intercomparisons, Characterization and Testing of Instruments and Method of Observation, Madrid, Spain, 27–29 September 2016.
8. Merlone, A.; Sanna, F.; Beges, G.; Bell, S.; Beltramino, G.; Bojkovski, J.; Brunet, M.; del Campo, D.; Castrillo, A.; Chiodo, N.; et al. The MeteoMet2 project—Highlights and results. *Meas. Sci. Technol.* **2017**, *29*, 025802. [CrossRef]
9. Coppa, G.; Quarello, A.; Steeneveld, G.; Jandrić, N.; Merlone, A. Metrological evaluation of the effect of the presence of a road on near-surface air temperatures. *Int. J. Clim.* **2021**, *41*, 3705–3724. [CrossRef]
10. Leeper, R.D.; Kochendorfer, J.; Henderson, T.A.; Palecki, M.A. Impacts of Small-Scale Urban Encroachment on Air Temperature Observations. *J. Appl. Meteorol. Clim.* **2019**, *58*, 1369–1380. [CrossRef]
11. The International System of Units (SI) 9th Edition 2019. Available online: https://www.bipm.org/en/publications/si-brochure (accessed on 25 January 2024).
12. Rezaei Rad, H.; Rafieian, M.; Sozer, H. Evaluating the effects of increasing of building height on land surface temperature. *Int. J. Urban Manag. Energy Sustain.* **2017**, *1*, 11–16. [CrossRef]
13. Peng, Y.; Gao, Z.; Ding, W. An approach on the correlation between urban morphological parameters and ventilation performance. *Energy Procedia* **2017**, *142*, 2884–2891. [CrossRef]
14. Guan, K. Surface and ambient air temperature associated with different ground material: A case study at the University of California, Berkeley. *Surf. Air Temp. Ground Mater.* **2011**, *196*, 1–14.
15. Brandsma, T.; Können, G.P.; Wessels, H.R.A. Empirical estimation of the effect of urban heat advection on the temperature series of De Bilt (The Netherlands). *Int. J. Clim.* **2003**, *23*, 829–845. [CrossRef]
16. Holmer, B.; Thorsson, S.; Eliasson, I. Cooling rates, sky view factors and the development of Intra-Urban air temperature differences. *Geogr. Ann. Ser. A, Phys. Geogr.* **2007**, *89*, 237–248. [CrossRef]
17. *EN 60751:2008*; Industrial Platinum Resistance Thermometers and Platinum Temperature Sensors. IEC: Geneve, Switzerland, 2007.
18. Nicholas, J.V.; White, D.R. Traceable Temperatures: An introduction to temperature measurement and calibration, 2nd edn. *Meas. Sci. Technol.* **2002**, *13*, 1651. [CrossRef]
19. Izquierdo, C.G.; Hernández, S.; González, A.; Matias, L.; Šindelářová, L.; Strnad, R.; del Campo, D. Evaluation of the self-heating effect in a group of thermometers used in meteorological and climate applications. *Meteorol. Appl.* **2019**, *26*, 117–129. [CrossRef]
20. Guide to the Realization of the ITS-90.BIPM/CCT:2018. Available online: https://www.bipm.org/documents/20126/41773843/Guide_ITS-90_5_SPRT_2021.pdf/c4bbbe56-4118-eef7-47cb-3ea234db40b8 (accessed on 25 January 2024).
21. Bristow, K.L.; Campbell, G.S. On the relationship between incoming solar radiation and daily maximum and minimum temperature. *Agric. For. Meteorol.* **1984**, *31*, 159–166. [CrossRef]
22. Prieto, J.; Martínez-García, J.; García, D. Correlation between global solar irradiation and air temperature in Asturias, Spain. *Sol. Energy* **2009**, *83*, 1076–1085. [CrossRef]
23. Bivand, R.S. Progress in the R ecosystem for representing and handling spatial data. *J. Geogr. Syst.* **2021**, *23*, 515–546. [CrossRef]
24. Dorman, M.; Erell, E.; Vulkan, A.; Kloog, I. Shadow: R Package for Geometric Shadow Calculations in an Urban Environment. *R J.* **2019**, *11*, 287–309. [CrossRef]
25. Kahle, D.; Wickham, H. ggmap: Spatial Visualization with ggplot2. *R J.* **2013**, *5*, 144–161. [CrossRef]
26. Hansen, P.C.; Pereyra, V.; Scherer, G. *Least Squares Data Fitting with Applications*; Johns Hopkins University Press: Baltimore, MD, USA, 2013.
27. White, D.R. Propagation of Uncertainty and Comparison of Interpolation Schemes. *Int. J. Thermophys.* **2017**, *38*, 39. [CrossRef]
28. White, D.R. The propagation of uncertainty with non-Lagrangian interpolation. *Metrologia* **2001**, *38*, 63–69. [CrossRef]
29. Koopmans, S.; Theeuwes, N.E.; Steeneveld, G.J.; Holtslag, A.A.M. Modelling the influence of urbanization on the 20th century temperature record of weather station De Bilt (The Netherlands). *Int. J. Clim.* **2014**, *35*, 1732–1748. [CrossRef]
30. Myrup, L.O. A Numerical Model of the Urban Heat Island. *J. Appl. Meteorol.* **1969**, *8*, 908–918. [CrossRef]
31. Kershaw, T.; Sanderson, M.; Coley, D.; Eames, M. Estimation of the urban heat island for UK climate change projections. *Build. Serv. Eng. Res. Technol.* **2010**, *31*, 251–263. [CrossRef]
32. Theeuwes, N.E.; Steeneveld, G.-J.; Ronda, R.J.; Holtslag, A.A.M. A diagnostic equation for the daily maximum urban heat island effect for cities in northwestern Europe. *Int. J. Clim.* **2017**, *37*, 443–454. [CrossRef]